Mustansiriyah Journal of Pure and Applied Sciences, Print ISSN: 2957-9910. Online ISSN: 2957-9929, Vol. 2, No. 4, 2024, Pages 140-156
DOI:

MJPAS

MUSTANSIRIYAH JOURNAL OF PURE AND APPLIED SCIENCES

Journal homepage*:*
https://mjpas.uomustansiriyah.edu.iq/index.php/mjpas

RESEARCH ARTICLE – **Atmospheric Science**

Effect of the density and height of F_2 layer on ground-based observation of jupiter's radio signal

Muhanad Hussien Khudhur[1*], Monim Hakim Al-Jiboori[2], Kamal Mohammed Abood[3]

[1,2]Atmospheric Science Department, College of Science, Mustansiriyah University, Baghdad, Iraq.

[3]Astronomy and Space Department, College of Science, University of Baghdad, Baghdad, Iraq.

*Corresponding author E-mail: *muhanad.hussien2005@gmail.com.

Article Info.

Article history:

Received
03 March 2024

Accepted
19 April 2024

Publishing
30 September 2024

Abstract

The observation of Jupiter's radio signals is affected by the density and height of the ionospheric F_2 layer. The study aims to determine an approximate observation threshold from the values of the F_2 peak density and the height of the F_2 peak. The study was conducted using data from the Florida and Lamy stations in the USA. Utilizing actual observation data of Jupiter's radio signals from the Radio JOVE Data Archive for the years 2014-2015. The Radio Jove Pro software was employed to predict radio emissions from Jupiter. Ionospheric data were sourced from the International Reference Ionosphere (IRI) website. The primary focus of this study is to examine the role of the ionosphere in blocking the radio signals emanating from Jupiter. It was found that 49% and 31% for the Florida and Lamy stations respectively of the predicted radio emission events from Jupiter were not observed. The likelihood of observation is higher after sunset and depends on Jupiter's elevation above the horizon relative to the observer. The F_2 peak density during nighttime and throughout the year ranged from approximately 10^{11} to 10^{12} m^{-3} at altitudes of about 260-360 km. 89% and 98% of the observations from the Florida and Lamy stations occurred when the F_2 peak density was less than around 6×10^{11} m^{-3}. In contrast, 80% and 56% (for the Florida and Lamy stations, respectively) of the cases of non-observation occurred when the F_2 peak density was greater than approximately 6×10^{11} m^{-3}. As for the height of the F_2 peak (hmF2), 85% and 93% of the observations from the Florida and Lamy stations occurred when the hmF_2 was greater than 300 km. The probability of observation is significantly influenced by the relationship between the ionospheric electron density and its corresponding altitude.

The official journal published by the College of Education at Mustansiriya University

Keywords: Ionosphere, Electron density, F_2 layer, Jupiter emission, Radio signal.

1. Introduction

Radio astronomy is the study of celestial bodies by examination of the radio-frequency energy they emit or reflect. Radio waves are able to pass through most of the gas and dust in space, as well as the clouds in planetary atmospheres, and they are a little affected when they travel through the Earth's atmosphere. As a result, radio astronomers are able to see stars and galaxies considerably more clearly than is feasible by optical observation. In the early 1930s, the concept of radio astronomy was born as a new and exciting branch of astronomy when extraterrestrial radio emissions from the Galaxy were first detected at 20 MHz [1].

Radio astronomers rely on short radio waves as the only way to penetrate the atmosphere and reach the ground. Frequencies between 5 MHz and 30 GHz are defined as the frequency bands that are able to get through the atmosphere, which are known as the radio windows. The window's low-frequency end is limited by the ionosphere's ability to reflect signals back into space, while its upper limit is determined by the atmosphere's ability to absorb radio waves. [2]. The atmosphere influences the transfer of radio waves. These waves are part of the electromagnetic spectrum, which extends from shorter to longer wavelengths [3]. Traveling radio waves interact with media through which they travel. Consequently, they can be reflected, refracted, or diffracted. These interactions may cause changes in the direction of radio signals. One of the most critical factors for radio waves is the ionospheric status [4]. Solar radiation constitutes the primary energy source reaching Earth. Sun releases energy into space in the form of electromagnetic radiation, which travels at the speed of light. This emission takes approximately 8 minutes to reach the outer atmosphere of Earth. The energy emanating from sun spans a broad range of wavelengths, extending from shorter lengths to longer wavelengths. It is categorized into three primary regions: the infrared radiation band (4 - 0.7 μm), the visible region (0.7 - 0.4 μm), which constitutes 44% of the solar spectrum, and the third main region known as the ultraviolet radiation band (0.4 - 0.2 μm) [5]. The ionosphere is the region of the Earth's atmosphere above 50 km in altitude where solar radiation is intense enough to ionize atoms and molecules of gases [6]. It contains ionized particles and atoms, free electrons, and neutral air particles. It is formed as a result of ionization due to short-wavelength solar radiation (UV and X-ray). In general, ionosphere can be divided into three distinct layers: D, E and F [7]. The D and E layers are found at a lower altitude, where the recombination rate of ions is extremely fast due to the high pressure, so the D and E layers disappear at night, but the F layer is found at a higher altitude where the pressure is lower so the recombination is very slow. Recombination is the opposite of ionization [8]. The highly ionized F layer is found at altitudes between 160 km and more than 500 km. The primary function of the F layer is the reflection of terrestrial radio waves back toward the ground, while concurrently impeding the penetration of extraterrestrial waves to reach the ground [6]. The ionization by solar radiation reaches its peak during local noon and in the summer, and increases as latitude decreases. Meanwhile, the layer's height is minimal during local noon and in the summer, and rises with higher latitudes [9]. Ionospheric activity is higher during the day due to increased ionization, but it weakens at night. Electron density and its height fluctuate in response to solar events. Solar flares occur during high solar activity, releasing large amounts of energy, heating the plasma, and emitting x-rays and ultraviolet rays that reach Earth's atmosphere. Solar flares are classified according to their X-ray fluxes into four categories: $B < 10^{-6}$ w/m^2, C=10^{-6}-10^{-5} w/m^2, M=10^{-5}-10^{-4} w/m^2 and $X > 10^{-4}$ w/m^2 [10]. Ultraviolet (UV) radiation, defined as electromagnetic radiation with wavelengths within the range of 100–400 nm, comprises 8.73% of the solar spectrum at the top of the atmosphere [11]. Ultraviolet radiation is usually classified into three bands: UVC = 100–280 nm, UVB = 280–315 nm, and UVA = 315–400 nm [12]. Ionization in the ionosphere is primarily induced by extreme ultraviolet (EUV) radiation with wavelengths below approximately 100 nm. Nearly half of the ionizing radiation power is concentrated at wavelengths below 27 nm [13]. Jupiter is one of the radio astronomical sources, it is emitting in frequency ranging from 10 kHz to 300 GHz. This emission is classified into four categories. kilometric (10-1000 kHz), Hectometric (1-3 MHz), Decametric (3-40 MHz), and Decimetric (0.1-300 GHz) [2]. Jovian radio emissions are difficult to detect during the daytime because these emissions are more likely to be covered by noise and less intense than solar emissions [14]. It is preferable to observe Jupiter's emissions in the absence of the sun when Jupiter is at a high peak position in the astronomical sky [15].

Jupiter's strongest radio emissions range from 50 kHz to 40 MHz. However, the Earth's ionosphere reflects frequencies below 15 MHz back into space. The preferred frequencies are 18–24 MHz because they are above the ionospheric cut-off frequency and not too close to man-made broadcast frequencies [16]. Depending on Jupiter's longitude, Jupiter's emissions are most likely found in three regions labeled A, B, and C, and certain orbital positions of it's moon (Io) led to enhanced emissions. These enhanced emissions are known as Io-A, Io-B, and Io-C. The ability to pick up Jupiter's emissions is influenced by several factors including: the state of the Earth's ionosphere, the relative position of the Earth and Jupiter in their orbits around the Sun, and the location of Jupiter relative to the observer on the Earth. [17].

1. Study Area

The location of the study was selected based on the availability of observational data for Jupiter's radio emissions. The study was conducted for the years 2014-2015 at two sites: The first site is the AJ4CO Observatory locates in High Springs, Florida, USA, situated at latitude 29.83° N, longitude 82.62° W, with an elevation of approximately 16 m above sea level. The AJ4CO Observatory is operated by Dave Typinski [18]. The second site is the Heliotown Observatory located in Lamy, Santa Fe, New Mexico, USA, located at latitude 35.29° N, longitude 105.53° W, with an elevation of about 1900 m above sea level. The Heliotown Observatory is operated by Thomas Ashcraft [19]. Both observatories primarily focus on radio astronomy, with a specific emphasis on Jupiter's radio emissions. The coordinates of both sites were mentioned by observers on the website of the Radio JOVE Data Archive (https://radiojove.net/query/inventory.php.). In this paper, the first site was referred to as (**Florida Station**) and the second site was referred to as (**Lamy Station**). Figure 1 displays the geographic locations of both study sites on the map.

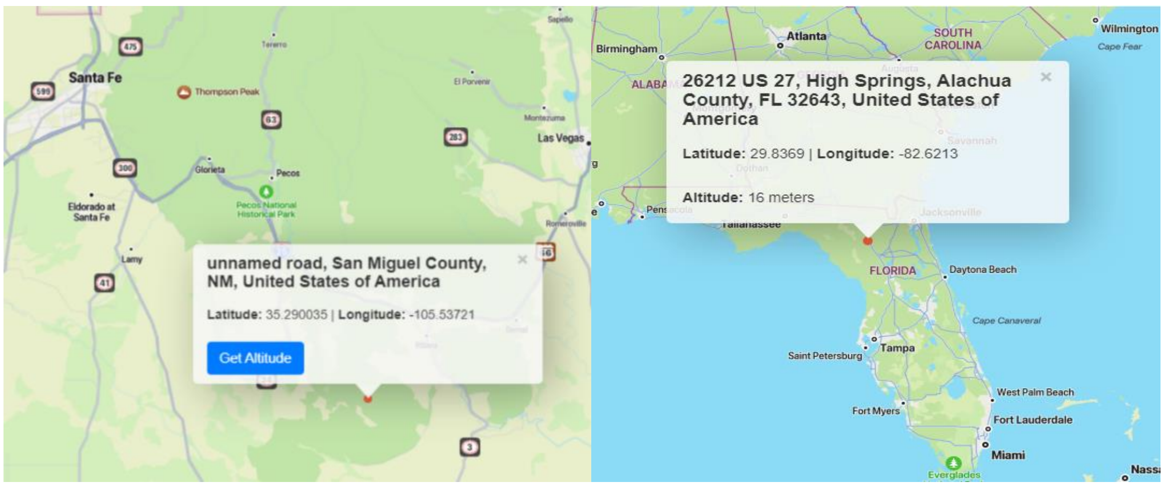

Fig. 1. The geographic locations of Florida and Lamy stations on the map. [20].

2. Data Sources

Two websites and one software program were utilized to collect data for this study, and they are described as follows:

2. 1 Radio JOVE Data Archive

The observations conducted by an astronomy group using the Radio Jove telescope at a frequency of 20.1 MHz for Jupiter and specific radio storm bursts are stored on the NASA website (http://radiojove.gsfc.NASA.gov). The data archive encompasses all observational data, including observer name, location (latitude and longitude), date, time, and storm type (see Figure 2). The archive of observations is accessible from 1999 to the present time. Regrettably, monitoring data is only intermittently available for years and stations, not continuously [21]. The study sites were selected based on the number of observations available in the data archive, with data from the years 2014-2015 being used.

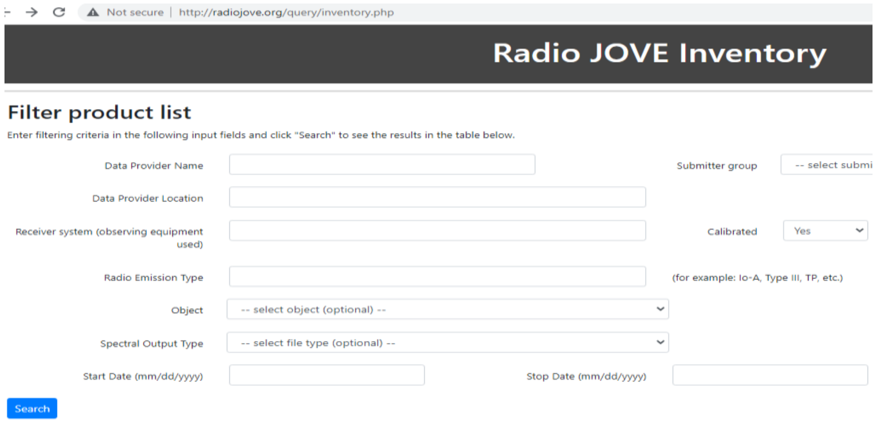

Fig. 2. Radio JOVE Data Archive website interface [21].

2.2 The International Reference Ionosphere

The International Reference Ionosphere (IRI) stands as a global model backed by the International Union of Radio Science (URSI) and the Committee on Space Research (COSPAR). In the late 1960s, these organizations collaborated to establish a working group tasked with creating an empirical standard model of the ionosphere, drawing upon all available data sources. The model has undergone several iterations, steadily improving over time. IRI provides monthly averages of electron density, electron temperature, ion temperature, and ion composition in the ionosphere, spanning altitudes from 60 to 2000 km, for specific locations, times, and dates (see Figure 3). Additional models and ionosphere-related data are regularly incorporated into the IRI [22]. Data for the model were sourced from ionosondes, incoherent scatter radars, topside sounder satellites, GPS, and rocket observations. However, in certain scenarios and specific timeframes, the accuracy of the IRI model may be compromised. Notably, the IRI effectively predicts the F layer of the ionosphere, primarily relying on GPS and ionosonde data. Conversely, the D and E layers, characterized by lower electron densities, are not as accurately captured using GPS or ionosonde data. This discrepancy underscores the lower accuracy of the D and E layer models, which are based on less data compared to the more robust F layer model [23].

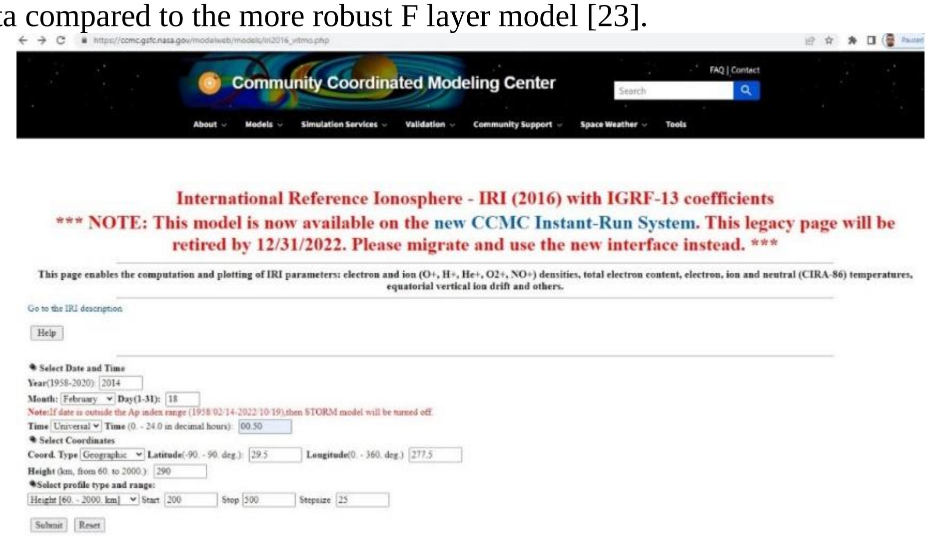

Fig. 3. International Reference Ionosphere website interface [22].

2.3 The Radio Jove Pro. Software

This program possesses specific features that aid in forecasting storms on the sun and Jupiter, planning observations, and tracking the motions of Jupiter and its moon, Io. It was designed for use by astronomers utilizing the Radio JOVE telescope (see Figure 4). This procedure was used to determine the expected number of Jupiter storms during the years 2014-2015 for both study sites [24].

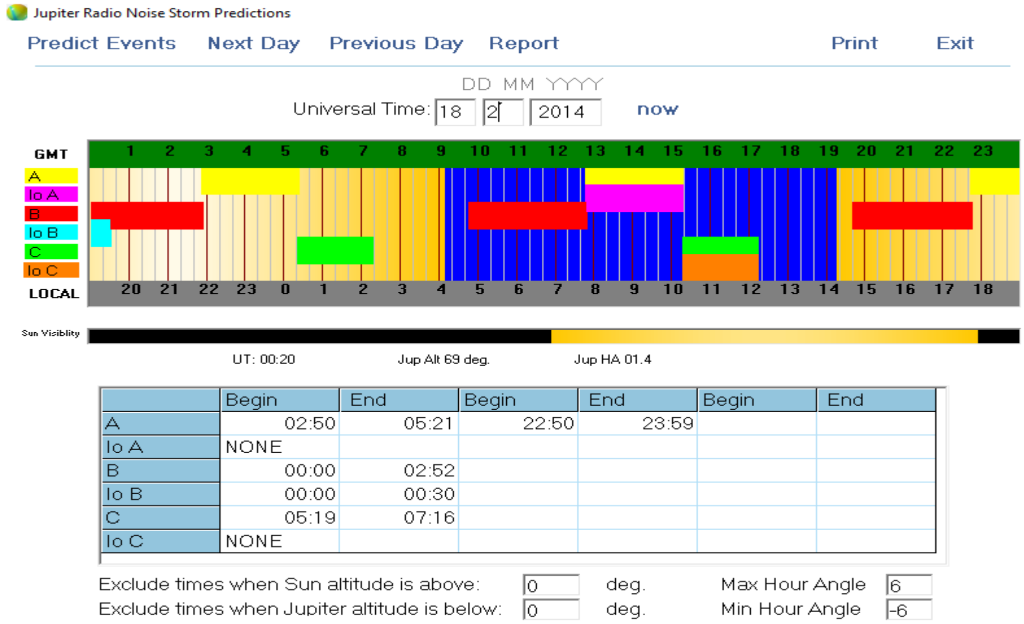

Fig. 4. The Radio Jove Pro. Software, Interface of Jupiter Radio Noise Storm Predictions [25].

3. Results and Discussion

For the years 2014-2015, and by using the Radio JOVE Pro software based on the movement of Jupiter and its satellite Io, there are about 240 events for Florida station and 218 events For Lamy station that refer to the likelihood that an observer would be able to detect a Jupiter radio storm using the Radio JOVE telescope. Due to the sun's higher radio emission density compared to Jupiter's, the likelihood of observing a Jupiter storm burst is minimal when the sun and Jupiter are both visible above the Earth's horizon at the same time, it is usually necessary to observe Jovian emissions well after dusk and before dawn.

From the Radio JOVE Pro software, the elevation of Jupiter and Sun above the horizon according to the location were obtained, and the actual observations were taken from Radio JOVE data archive of Florida and Lamy stations. Events were filtered by excluding those in which the Sun was above the Earth's horizon and Jupiter's elevation was below the Earth's horizon. This filtering process resulted in a reduction in the number of events, as illustrated in the table 1.

Table 1. The dates of predicted events and actual observations for Florida and Lamy stations of years 2014 and 2015.

Station	Year	Predicted events	Predicted events after Filtering	Actual Observations	Predicted unobserved events
Florid	2014	116	50	33	17

a	2015	124	41	13	28
	SUM.	240	91	46	45
Lamy	2014	107	40	20	20
	2015	111	45	38	7
	SUM.	218	85	58	27

From the table 1, about 49% and 31% (for the Florida and Lamy stations, respectively) of the predicted radio emission events from Jupiter were not observed. The height of the F_2 peak (hmF_2) and the density of the F_2 peak (NmF_2) data were taken from IRI. Using the OriginLab2021 program, the NmF_2 and hmF_2 were plotted for the times 00:00, 06:00 and 12:00 UTC which represented the night period along the year. Figures 5-6 show that hmF_2 during the night ranges between approximately 260 and 360 km, and the NmF_2 ranges between 10^{11} and 10^{12} m^{-3}. It was noted that the highest NmF_2 (at night) was at 00:00 UTC in the spring, and the lowest NmF_2 was at 06:00 UTC in the winter.

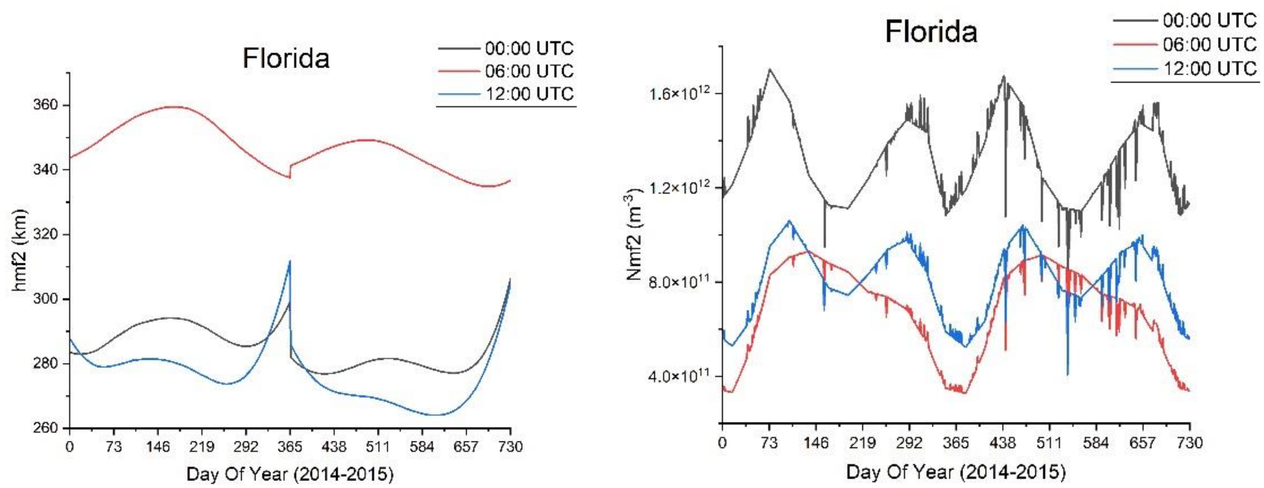

Fig. 5. Represents NmF_2 and hmF_2 during the night throughout the years 2014-2015, for Florida station, local time =UTC-5.

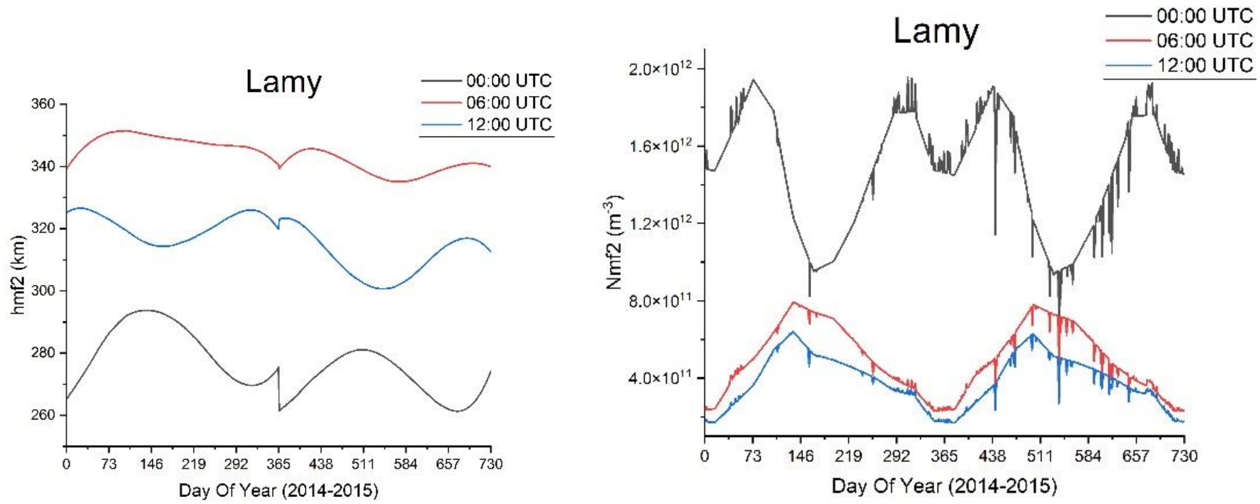

Fig. 6. Represents NmF_2 and hmF_2 during the night throughout the years 2014-2015, for Lamy station, local time =UTC-7.

It is noted that the hmF_2 is inversely related to NmF_2. So, the highest hmF_2 was accompanied by the lowest value of NmF_2 at 06:00 UTC, and the lowest hmF_2 was at 00:00 UTC (near sunset) and 12:00 UTC (near sunrise) and accompanied by the highest value of NmF_2. The predicted unobserved events (UN-OBS) were taken from the Radio JOVE Pro software, and the actual observations (OBS) were taken from Radio JOVE data archive. The hmF_2 and NmF_2 data were taken from IRI and were tabulated according to date for the Florida station in Table 2 and the Lamy station in Table 3.

0

Table 2. The dates of predicted unobserved events (UN-OBS) and actual observations (OBS) for Florida station of the years 2014 and 2015.

OBS Date	UN-OBS Date	Time	Jupiter altitude	Sun altitude	Height of F_2 peak	Density of F_2 peak	Storm type
dd/mm/yyyy	dd/mm/yyyy	UTC	angle	angle	hmF2(km)	NmF2(m^{-3})	
01/01/2014		03:40	58.5	-65.5	330.9	4.450E+11	Io-B
05/01/2014		06:53	71.85	-69.7	342.8	2.158E+11	Io-A
06/01/2014		10:22	25.9	-24.8	326.3	2.452E+11	Io-B
09/01/2014		02:42	53.8	-51.8	322.7	5.776E+11	Io-A
12/01/2014		07:45	53.9	-58.8	342.8	3.657E+11	Io-A
16/01/2014		03:24	69.7	-59.9	331.9	2.340E+11	Io-A
17/01/2014		04:36	82.6	-74.2	341.5	2.005E+11	Io-B
23/01/2014		04:13	83.04	-68.9	340.2	2.284E+11	Io-A/C
24/01/2014		04:20	83	-70.3	341.2	2.288E+11	Io-B
30/01/2014		03:40	83.08	-61.18	337.2	2.685E+11	Io-A/C
31/01/2014		05:03	70.81	-75.81	345.3	2.427E+11	Io-B
06/02/2014		03:02	82.6	-52.03	331.8	3.224E+11	Io-A/C
07/02/2014		06:13	49.1	-73.85	347.6	4.747E+11	Io-B
13/02/2014		03:44	75.41	-59.47	340.2	3.153E+11	Io-A
	18/02/2014	00:30	63.31	-17.3	290.7	6.818E+11	IO-B
	23/02/2014	23:59	61.8	-9.5	284.8	8.491E+11	IO-A
	24/02/2014	00:57	74	-22	299.1	6.760E+11	IO-A/C
25/02/2014		01:56	83.45	-34.93	317.9	5.045E+11	Io-B
	02/03/2014	23:59	68	-8.5	285.8	8.553E+11	IO-A
03/03/2014		01:30	83.45	-28.44	310.5	5.946E+11	Io-C
04/03/2014		01:16	82.91	-25.26	305.9	6.377E+11	Io-B
	09/03/2014	23:59	73.7	-7.5	286.8	9.065E+11	IO-A
10/03/2014		01:04	83.48	-21.8	302.7	7.075E+11	Io-C
11/03/2014		02:22	70.62	-38.16	327.3	5.312E+11	Io-B
	17/03/2014	00:36	83.46	-14.76	295.3	8.324E+11	IO-A/C
	19/03/2014	01:38	73.44	-27.71	315	6.566E+11	IO-A
	24/03/2014	01:45	68	-28	317.9	6.572E+11	IO-A
04/04/2014		23:57	80.6	-3.99	289.9	9.909E+11	Io-B
	05/04/2014	00:00	80.27	-4.42	290.4	9.843E+11	IO-B
	10/04/2014	23:57	76.77	-3.2	290.6	1.000E+12	IO-C
11/04/2014		23:57	76.09	-3.07	290.7	1.003E+12	Io-B
	12/04/2014	00:00	75.69	-3.5	291.2	9.967E+11	IO-B

	18/04/2014	00:06	70.18	-3.98	292.5	9.770E+11	IO-C
26/04/2014		23:57	65.39	-1.09	292	9.699E+11	Io-A
	27/04/2014	00:00	64.9	-1.51	292.4	9.603E+11	IO-A
	03/05/2014	23:57	60.3	-0.17	292.7	9.418E+11	IO-A
18/10/2014		11:22	62.38	-1.6	296.3	4.204E+11	Io-B
	26/10/2014	10:54	62.01	-8.74	311.4	3.201E+11	IO-A
02/11/2014		11:33	72.54	-1.69	293.6	4.248E+11	Io-A
09/11/2014		11:39	75.09	-1.55	292.5	4.297E+11	Io-A
16/11/2014		11:34	75.02	-3.52	297.6	4.263E+11	Io-A
	23/11/2014	11:32	73.22	-5.07	301	3.566E+11	IO-A
	26/11/2014	09:02	61.26	-37.34	330.8	2.336E+11	IO-B
05/12/2014		08:48	65.07	-41.62	326.7	2.281E+11	Io-B
11/12/2014		08:46	68.8	-42.85	323.7	2.186E+11	Io-A/C
12/12/2014		09:48	74.97	-29.62	325.3	1.766E+11	Io-B
18/12/2014		09:28	74.98	-34.66	322.2	1.780E+11	Io-A/C
19/12/2014		09:44	73.94	-31.35	322.9	1.692E+11	Io-B
25/12/2014		08:48	75.07	-44.08	316	2.034E+11	Io-A/C
26/12/2014		10:33	62	-21.9	323.9	1.768E+11	Io-B
01/01/2015		08:24	75.3	-49.95	334.8	3.432E+11	Io-A
03/01/2015		10:00	62.03	-29.36	328.3	2.611E+11	Io-A
06/01/2015		04:55	44.21	-79.68	340.2	3.501E+11	Io-B
12/01/2015		04:53	49.38	-78.39	340.9	3.451E+11	Io-A/C
13/01/2015		06:39	70.93	-72.79	341.2	3.422E+11	Io-B
19/01/2015		06:59	75.77	-68.65	341.2	3.703E+11	Io-A/C
20/01/2015		07:15	75.67	-65.31	340.9	3.798E+11	Io-B
26/01/2015		06:35	76.17	-72.82	342.6	3.988E+11	Io-A/C
27/01/2015		06:31	76.22	-73.4	342.8	4.171E+11	Io-B
02/02/2015		06:01	76.43	-76.98	343.9	4.732E+11	Io-A/C
03/02/2015		08:12	57.26	-52.57	342.1	4.619E+11	Io-B
04/02/2015		06:07	76.36	-75.34	344	4.551E+11	Io-A
09/02/2015		05:37	76.76	-75.53	344.7	4.847E+11	Io-A
	11/02/2015	06:49	66.79	-67.65	344.2	4.940E+11	Io-A
	21/02/2015	04:11	75.43	-62.66	341.6	6.283E+11	Io-B
	27/02/2015	02:24	61.72	-40.63	321.3	8.821E+11	Io-A/C
	28/02/2015	04:15	77.47	-61.56	342.2	6.996E+11	Io-B
	06/03/2015	03:30	77.29	-52.53	336.1	8.095E+11	Io-A/C
	07/03/2015	04:03	76.69	-57.83	341	7.897E+11	Io-B
	08/03/2015	02:26	69.92	-39.55	322.1	9.788E+11	Io-A

	13/03/2015	04:57	63.63	-62.54	345.7	8.208E+11	Io-A/C
	15/03/2015	03:00	77.87	-45	330.1	9.531E+11	Io-A
	20/03/2015	03:14	76.23	-46.51	333.2	9.085E+11	Io-A
	22/03/2015	03:40	71.09	-50.41	337.5	9.330E+11	Io-A
	31/03/2015	00:32	66.79	-12.01	285	1.457E+12	Io-C
	01/04/2015	01:36	77.39	-25.26	305.9	1.234E+12	Io-B
	07/04/2015	01:14	77.57	-19.8	298.6	1.300E+12	Io-C
	08/04/2015	01:20	78.09	-20.86	299.6	1.292E+12	Io-B
	13/04/2015	23:57	70.85	-2.85	278.5	1.558E+12	Io-A
	14/04/2015	01:10	78.11	-17.88	296.5	1.315E+12	Io-C
	15/04/2015	02:02	71.49	-27.89	314.4	1.215E+12	Io-A/B
	16/04/2015	00:28	76.55	-8.92	284	1.317E+12	Io-A
	21/04/2015	00:32	78.09	-9.04	285.7	1.369E+12	Io-A
	23/04/2015	00:26	78.09	-7.52	284.4	1.370E+12	Io-A
	28/04/2015	01:22	69.75	-17.96	300.6	1.223E+12	Io-A
	30/04/2015	00:42	75.09	-9.77	288.4	1.281E+12	Io-A
	08/12/2015	11:48	64.61	-4.12	293.6	2.533E+11	Io-B
	14/12/2015	10:50	62.64	-16.76	313.1	1.406E+11	Io-A/C
	15/12/2015	11:06	63.92	-13.58	310.7	1.663E+11	Io-B
	21/12/2015	11:32	63.53	-8.99	306.7	1.950E+11	Io-A/C
	28/12/2015	10:30	64.08	-22.49	316	1.119E+11	Io-A

Table 3. The dates of predicted unobserved events (UN-OBS) and actual observations (OBS) for Lamy station of years 2014 and 2015.

OBS Date	UN-OBS Date	Time	Jupiter altitude	Sun altitude	Height of F_2 peak	Density of F_2 peak	storm type
dd/mm/yyyy	dd/mm/yyyy	UTC	angle	angle	hmF2(km)	NmF2(m^{-3})	
	05/01/2014	06:53	76.65	-77.24	346	2.223E+11	Io-A
	07/01/2014	08:30	66.99	-66.85	348.4	2.726E+11	Io-A
12/01/2014		07:45	70.8	-73.63	349.5	2.401E+11	Io-A
	17/01/2014	04:35	64.46	-54.18	330	3.696E+11	Io-B
21/01/2014		09:54	37.8	-50.35	350.1	2.927E+11	Io-A
23/01/2014		04:05	63.89	-47.15	324.7	4.681E+11	Io-A
24/01/2014		05:51	77.45	-66.92	343.9	2.933E+11	Io-B
	30/01/2014	04:49	75.95	-54.59	334.8	4.058E+11	Io-A/C
31/01/2014		05:15	77.6	-59.26	339.9	3.686E+11	IO-B
06/02/2014		05:31	74.57	-60.75	343.3	3.837E+11	Io-C
07/02/2014		06:13	67.05	-66.68	348.6	3.607E+11	Io-B
	08/02/2014	04:39	77.68	-50.9	334.4	4.864E+11	Io-A
13/02/2014		04:15	77.7	-45.27	329.5	5.471E+11	Io-A
14/02/2014		08:00	39.91	-65.47	355.5	4.093E+11	Io-B
	15/02/2014	05:23	69.94	-57.28	343.6	4.382E+11	Io-A
20/02/2014		05:25	65.83	-56.36	344.2	4.461E+11	Io-A
22/02/2014		06:05	56.4	-61.39	349.9	4.354E+11	Io-A
01/03/2014		06:49	41.65	-62.46	354.2	4.357E+11	Io-A
03/03/2014		02:46	77.21	-24.32	306.6	9.655E+11	Io-A/C
	04/03/2014	02:40	77.07	-22.92	304.9	1.001E+12	Io-B
	10/03/2014	01:46	73.61	-10.87	292.2	1.334E+12	Io-A/C
	11/03/2014	02:30	77.82	-19.64	302.9	1.076E+12	Io-B
	17/03/2014	03:24	69.67	-29.17	318.7	8.281E+11	Io-A/C
	19/03/2014	02:08	77.75	-13.77	297.3	1.229E+12	Io-A
	24/03/2014	01:50	77.72	-9.25	294.4	1.309E+12	Io-A
	26/03/2014	02:24	73.9	-15.73	302.2	1.128E+12	Io-A
	12/04/2014	01:24	73.73	-0.81	291.9	1.410E+12	Io-B
	19/04/2014	01:50	65.15	-4.82	296.1	1.240E+12	Io-B
	25/10/2014	12:47	62.08	-5.32	303.6	4.765E+11	Io-B
	03/11/2014	12:19	62.3	-12.52	319	3.575E+11	Io-B
09/11/2014		12:35	67.05	-10.36	312.4	4.024E+11	Io-A/C
10/11/2014		12:47	68.43	-8.16	307.3	4.814E+11	Io-B
	16/11/2014	13:17	69.05	-3.4	294.8	6.232E+11	Io-A/C

23/11/2014		12:15	69.06	-16.77	321.9	2.939E+11	Io-A
	30/11/2014	12:15	69.22	-17.92	322.2	2.589E+11	Io-A
	12/12/2014	10:38	67.43	-39.06	325.1	2.209E+11	Io-B
18/12/2014		09:28	61.65	-54.08	324.3	2.809E+11	Io-A/C
19/12/2014		10:30	68.89	-41.57	320.1	2.224E+11	Io-B
25/12/2014		10:10	69.18	-46.29	315.6	2.476E+11	Io-A/C
26/12/2014		10:34	69.33	-41.48	314.6	2.337E+11	Io-B
01/01/2015		10:00	69.64	-48.9	338	1.58E+11	Io-A/C
02/01/2015		12:19	51.54	-20.99	317.8	1.20E+11	Io-B
03/01/2015		10:00	69.55	-49.02	338.9	1.69E+11	Io-A
08/01/2015		09:52	69.11	-50.87	341.3	1.70E+11	Io-A/C
10/01/2015		10:42	62.55	-40.72	338.4	1.28E+11	Io-A
12/01/2015		05:13	33.59	-62.46	334.9	1.46E+11	Io-A/C
17/01/2015		11:24	49.91	-32.16	333.3	1.08E+11	Io-A
19/01/2015		06:59	60.08	-75.22	347.2	1.36E+11	Io-A/C
20/01/2015		08:24	70.12	-67.37	347.7	1.65E+11	Io-B
24/01/2015		12:05	35.96	-23.74	321.2	1.22E+11	Io-A
26/01/2015		08:12	70.52	-68.5	348.9	1.78E+11	Io-A/C
27/01/2015		08:00	70.54	-69.96	349.1	1.84E+11	Io-B
02/02/2015		07:25	70.63	-71.57	349.7	2.00E+11	Io-A/C
03/02/2015		08:12	69.05	-67	350.2	2.22E+11	Io-B
09/02/2015		07:05	71.12	-69.84	286.9	5.38E+11	Io-A/C
10/02/2015		09:56	47.01	-47.64	349.3	2.17E+11	Io-B
11/02/2015		06:49	71.11	-68.72	349.4	2.11E+11	Io-A
18/02/2015		07:31	66.52	-66.38	351.7	2.41E+11	Io-A
25/02/2015		08:12	54.7	-60.69	353.2	2.51E+11	Io-A
27/02/2015		04:19	63.23	-43.22	326.4	3.02E+11	Io-A/C
04/03/2015		08:54	40.45	-52.76	353.9	2.49E+11	Io-A
06/03/2015		05:03	71.8	-49.3	336	2.74E+11	Io-A/C
13/03/2015		04:57	72.08	-46.51	334.2	2.88E+11	Io-A/C
15/03/2015		04:13	71.42	-38.58	323.8	3.30E+11	Io-A
	22/03/2015	04:05	72.4	-35.56	321.2	3.53E+11	Io-A
29/03/2015		04:23	70.03	-36.95	325	3.45E+11	Io-A
	01/04/2015	01:54	62.95	-8.74	284.1	6.65E+11	Io-B
05/04/2015		05:07	58.94	-41.5	333.9	3.22E+11	Io-A/C
	07/04/2015	01:16	60.52	-0.07	278.1	7.75E+11	Io-C
08/04/2015		02:38	71.95	-16.14	295.4	5.57E+11	Io-B
	14/04/2015	02:00	70.85	-7.68	285.3	6.66E+11	Io-C

	23/04/2015	02:00	72.47	-6.13	285.2	6.59E+11	Io-A
	28/04/2015	01:34	72.3	-0.25	280.6	7.05E+11	Io-A
07/05/2015		03:56	48.92	-23.65	314.7	4.56E+11	Io-A/C
08/05/2015		04:11	45.38	-25.46	318.1	4.50E+11	Io-B
	14/05/2015	02:12	63.45	-4.89	287.9	5.21E+11	Io-A/C
05/11/2015		13:15	49.08	-1.69	284.6	2.80E+11	Io-A
12/11/2015		13:23	53.38	-1.45	283.2	2.66E+11	Io-A
07/12/2015		10:32	38.83	-39.54	317.5	1.24E+11	Io-A/C
14/12/2015		12:25	57.52	-17.95	313.1	1.16E+11	Io-A/C
15/12/2015		12:25	57.72	-18.08	313.5	1.14E+11	Io-B
21/12/2015		12:15	58.17	-20.75	314.5	9.79E+10	Io-A/C
22/12/2015		12:25	58.54	-18.89	314.1	1.03E+11	Io-B
28/12/2015		13:07	56.03	-11.28	310.5	1.32E+11	Io-A/C
30/12/2015		11:40	58.03	-28.37	310	7.87E+10	Io-A

The data in Tables 2 and 3 are displayed with histograms of NmF_2 and hmF_2 frequencies for both observed and unobserved cases and shown Figures 7 and 8.

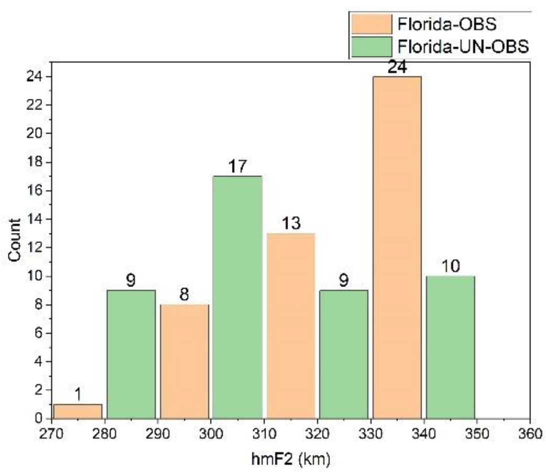

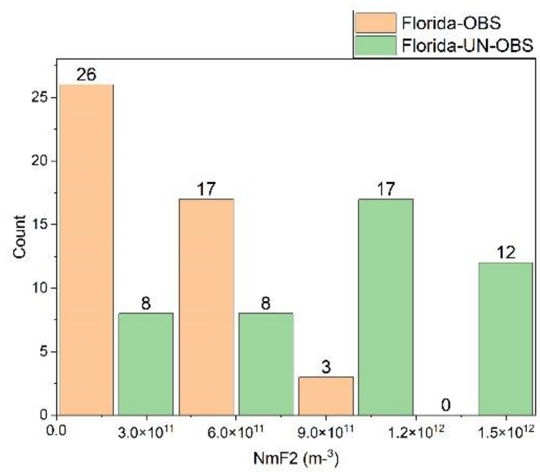

Fig. 7. Histograms for both of observed (OBS) and unobserved (UN-OBS) cases show the height of the F_2 peak (hmF_2) and F_2 peak density (NmF_2) for Florida station.

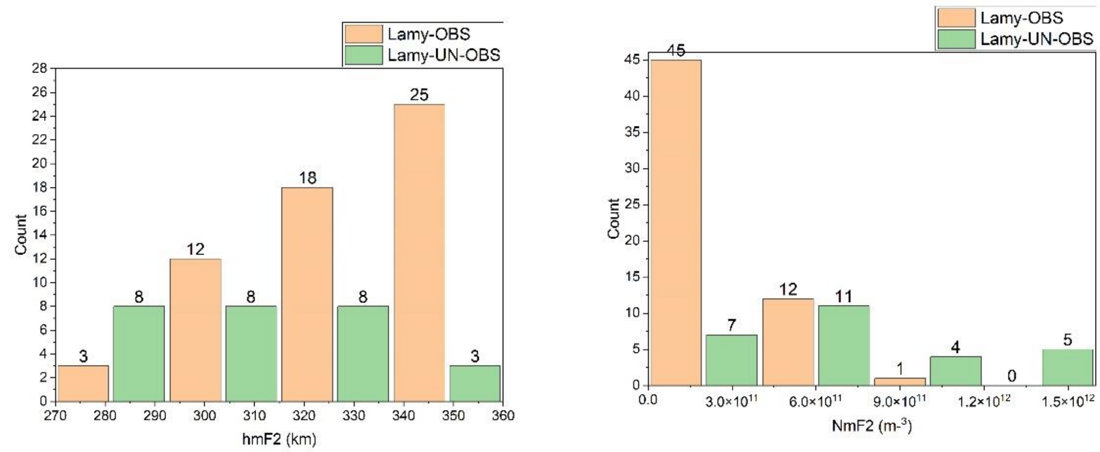

Fig. 8. Histograms for both of observed (OBS) and unobserved (UN-OBS) cases show the height of the F_2 peak (hmF_2) and F_2 peak density (NmF_2) for Lamy station.

The data were analyzed and classified according to the density of the F_2 peak (NmF_2) and the height of the F_2 peak (hmF_2). The results were displayed in the form of percentages representing the probability of observation (see Tables 4-5).

Table 4. The probability of observation, expressed as a percentage, has been classified according to the height of the F_2 peak (hmF_2) and the density of the F_2 peak (NmF_2) for predicted unobserved events and actual observations for Florida station of years 2014-2015.

Florida station	Cases number	NmF_2 (m^{-3})	Percentage %	Cases number	hmF_2 (km)	Percentage %
46 observed cases	5	6.38×10^{11} – 1.00×10^{12}	11	7	290-287.6	15
	41	1.69×10^{11} - 5.95×10^{11}	89	39	302.7-347.6	85
45 predicted unobserved cases	9	1.12×10^{11} - 4.94×10^{11}	20	23	300.6-345.7	51
	36	6.28×10^{11} – 1.56×10^{12}	80	22	278.5-299.6	49

Table 5. The probability of observation, expressed as a percentage, has been classified according to the height of the F_2 peak (hmF_2) and the density of the F_2 peak (NmF_2) for predicted unobserved events and actual observations for Lamy station of years 2014-2015.

Lamy station	Cases number	NmF_2 (m^{-3})	Percentage %	Cases number	hmF_2 (km)	Percentage %
58 observed cases	1	9.655×10^{11}	2	4	283.2-295.4	7
	57	7.87×10^{10} - 5.57×10^{11}	98	54	306.6-355.5	93
27 predicted	12	2.2×10^{11} –	44	15	302.2-	56

unobserved cases		5.21×10^{11}			348.4	
	15	6.23×10^{11} – 1.41×10^{12}	56	12	278.1-297.3	44

An approximate observation threshold can be determined from the values of NmF_2 and hmF_2 based on their recurrence. According to the results from Figures 7-8 and Tables 4-5, it was noted that 89% of the observations occurred when the F_2 peak density was less than approximately 6×10^{11} m^{-3} for the Florida station and the percentage increased to 98% for the Lamy station. 80% of the cases of non-observation occurred when the F_2 peak density was greater than approximately 6×10^{11} m^{-3} for Florida station but it decreased to 56% for Lamy station. As for hmF_2, 85% and 93% of the observations occurred when the hmF2 was greater than about 300 km for the Florida and Lamy stations, respectively.The highest recurrence for the observed cases was for hmF_2 greater than 300 km and NmF_2 less than 6×10^{11} m^{-3}, while the highest recurrence for the predicted unobserved cases was for hmF_2 less than 300 km and NmF_2 greater than 6×10^{11} m^{-3} for both of Florida and Lamy stations.The approximate observation threshold should be less than 6×10^{11} m^{-3} for Nmf2 and greater than 300 km for hmF_2.

4. Conclusions

A significant percentage of Jupiter's radio emissions have not been observed due to being blocked by the ionosphere. The ability to observe Jupiter's radio emissions is enhanced after sunset and depends on Jupiter's elevation above the horizon in relation to the observer.
The F2 Peak Density (NmF2) varies between 10^{11} and 10^{12} m^{-3} during the night at an altitude of approximately 260-360 km. The height of the F_2 peak is inversely related to the density of the F_2 peak, and the likelihood of Jovian radio emission observation is significantly influenced by the electron density and its altitude. Observation probability increases with lower electron density and at higher altitudes whereas it decreases with higher electron density and at lower altitudes.
The ionosphere has an impact on the observation of Jupiter's radio signal, at least up to an altitude of 300 km and with an electron density exceeding 6×10^{11} m^{-3}.

6. References

[1] W. Orchiston, P. Robertson and W. T. Sullivan III, Golden Years of Australian Radio Astronomy: An Illustrated History, Springer Nature, 2021.

[2] J. Thieman, C. Higgins and L. Garcia, "The Effects of Earth's Upper Atmosphere on Radio Signals," [Online]. Available: https://radiojove.gsfc.nasa.gov/education/lesson_plans/complete.pdf. [Accessed Feb. 11, 2023].

[3] H. A. Nemah, M. M. Ahmed, O. L. Khaleed and G. S. Nemat, "Effect of Some Meteorological Variables and Conditions on Mobile Phone and TV Satellite Signal," *Al-Mustansiriyah Journal of Science*, vol. 32, no. 2, pp. 71-75, 2021.

[4] K. A. Hadi, "Mutual Correlation Between MUF and FOT Parameters at Baghdad for the Maximum Solar Cycle 23," *Al-Mustansiriyah Journal of Science,* vol. 22, no. 4, pp. 308-319, 2011.

[5] B. A. Al-Knani, I. H. Abdulkareem, H. A. Nemah and Z. Nasir, "Studying the Changes in Solar Radiation and Their Influence on Temperature Trend in Iraq for a Whole Century," *Baghdad Science Journal,* vol. 18, no. 2, pp. 1076-1080, 2021.

[6] M. C. Kelley, The earth Ionosphere: Plasma Physics and Electrodynamics, 2nd ed., san diego: Academic Press, 2009, pp. 1-6.

[7] S. A. Thabit, L. E. George and K. A. Hadi, "Seasonal Variations of the Optimum Reliable Frequencies during Maximum and Minimum Periods of Solar Cycle 24," *Al-Mustansiriyah Journal of Science,* vol. 31, no. 4, pp. 15-27, 2020.

[8] M. M. S. Al-gubory, *"Investigating the Validity of the IRI Model for the Total Electron Content During Strong, Sever and Great Geomagnetic Storms,",* M.S. thesis, Dept. Astronomy and Space, Univ. Baghdad, Baghdad, Iraq, 2015.

[9] A. D. al-Jubouri, *"The phenomenon of the F layer spread in the ionosphere over the city of Baghdad,",* M.S. thesis, Dept. Atmospheric Sciences, Univ. Al-Mustansiriyah, Baghdad, Iraq, 2002.

[10] R. S. Al-Awadi, O. T. Al-Taai and S. A. Abdullah, "Assessment of X-Ray Effects on HF Radio Communications," *IOP Conference Series: Earth and Environmental Science,* vol. 1223, no. 1, 2023.

[11] O. T. Al-Taai, I. K. Al-Ataby and B. A. Al-Knani, "IMPACT OF SOME ATMOSPHERIC FACTORS ON ULTRAVIOLET RADIATION FOR SELECTED MONITORING STATIONS IN IRAQ," *Plant Archives,* vol. 20, no. 1, pp. 47-55, 2020.

[12] A. M. Alsalihi and S. H. Abdulatif, "Analysis Global and Ultraviolet Radiation in Baghdad City, Iraq," *Journal of Natural Sciences Research,* vol. 6, no. 22, pp. 117-124, 2016.

[13] W. K. Peterson, T. N. Woods and J. M. Fontenla, "Solar EUV and XUV energy input to thermosphere on solar rotation time scales derived from photoelectron observations," *Journal of Geophysical Research: Space Physics,* vol. 117, no. A5, 2012.

[14] N. M. Ebadi and K. M. Abood, "Study of Sunspot Effect on Radio Jove Telescope Observation," *Iraqi Journal of Science,* vol. 55, no. 1, pp. 258-267, 2014.

[15] H. U. Alaa-AlDeen and K. M. Abood, "Study of Actual Jupiter Observation Days at UFRO Station During 2004 Year," *Iraqi Journal of Science,* vol. 57, no. 1c, pp. 768-774, 2016.

[16] M. H. Khudhur, M. H. Al-Jiboori and K. M. Abood, "The study of the effect of Ionospheric variables on the astronomical radio signal," *Accepted by Iraqi Journal of Science,* vol. 65, no. 11, 2023.

[17] W. D. Reeve, "Listening to Jupiter's Radio Storms Part 1," *Journal of radio user,* vol. 1, no. 1, pp. 32-37, 2009.

[18] D. Typinski, "AJ4CO Observatory," [Online]. Available: https://www.aj4co.org/index.html.

[Accessed Feb. 29, 2023].

[19] T. Ashcraft, "Heliotown Observatory," [Online]. Available: https://www.heliotown.com/. [Accessed Sep. 12, 2023].

[20] "GPS Coordinates and Maps," gps-coordinates.net, [Online]. Available: https://www.gps-coordinates.net/. [Accessed Jan. 20, 2023].

[21] "Radio JOVE Data Archive," Radio JOVE Project, [Online]. Available: https://radiojove.net/query/inventory.php. [Accessed Jan. 18, 2023].

[22] "International Reference Ionosphere - IRI (2016) with IGRF-13 coefficients," Community Coordinated Modeling Center, [Online]. Available: https://ccmc.gsfc.nasa.gov/modelweb/models/iri2016_vitmo.php. [Accessed Dec. 25, 2022].

[23] D. Bilitza, L.-A. McKinnell, B. Reinisch and T. Fuller-Rowell, "The international reference ionosphere today and in the future," *Journal of Geodesy*, vol. 85, no. 12, pp. 909-920, 2011.

[24] R. S. Flagg, Listening to Jupiter: A Guide for the Amateur Radio Astronomer, 2nd ed., Louisville, Kentucky: Radio-Sky Publishing, 2000, pp. 28-29.

[25] Radio-Jupiter Pro 3. (2001). Radio Sky Publishing. Accessed: Nov. 15, 2022, [Online]. Available: https://radiosky.com/rjpro3ishere.html.